Soft Matter

Cite this: *Soft Matter*, 2012, **8**, 8361

www.rsc.org/softmatter

PAPER

Amphiphilic hyperbranched copolymers bearing a hyperbranched core and dendritic shell: synthesis, characterization and guest encapsulation performance†

Yi Liu,[a] You Fan,[a] Xun-Yong Liu,[b] Song-Zi Jiang,[a] Yuan Yuan,[a] Yu Chen,*[a] Fa Cheng[a] and Shi-Chun Jiang*[c]

Received 29th March 2012, Accepted 29th May 2012
DOI: 10.1039/c2sm25732g

The 2,2-bis(hydroxymethyl)propionic acid (BHP)-based generation 1 dendron with two palmitate tails (D1-C16) and the generation 2 dendron with four palmitate tails (D2-C16) were synthesized. The coupling of D1-C16 or D2-C16 with hyperbranched polyethylenimine (PEI) through the amidation reaction resulted in amphiphilic hyperbranched copolymers bearing a hyperbranched PEI core and a dendritic D1-C16 shell or dendritic D2-C16 shell. The structure of the obtained copolymers was verified through Fourier transform infrared (FTIR) and ^{1}H nuclear magnetic resonance (NMR) characterization. Differential scanning calorimetry (DSC) measurement demonstrated that the existence of the branching units in the shell pronouncedly reduced the crystallinity of the hyperbranched copolymers, and the copolymers with less branched shells had a higher melting temperature and melting enthalpy. These novel amphiphilic hyperbranched copolymers could be used as nanocarriers to efficiently accommodate the hydrophilic guests, including Methyl Orange (MO), Congo Red (CR) and Direct Blue 15 (DB), into the hydrophilic amidated PEI core. Each nanocarrier with a branched shell could accommodate a much higher number of guests than the corresponding nanocarriers with linear shells, which indicated that the dendritic structure of the shell played a key role in significantly enhancing the encapsulation capacity of the nanocarriers. As far as the weight ratio of the encapsulated guests to the nanocarriers was concerned, the nanocarriers with branched shells could be modulated to have a similar encapsulation capacity for the small MO with a mono-sulfonate group, but a much superior encapsulation capacity for the large CR and DB guests with multi-sulfonate groups to the nanocarriers with linear shells.

Introduction

Dendritic polymers have attracted tremendous interest due to their specific spheroid-like shape and multi-functionality, which are powerful motifs in the design of new molecular and supramolecular structures.[1–3] Through the hybridization of dendritic and linear polymers, various copolymers have been prepared,[3–7] such as multiarm star copolymers, linear–dendritic hybrid copolymers, dendronized copolymers, and dendrigraft copolymers. However, copolymers consisting of only two different dendritic polymeric segments are very scarce. Wooley *et al.* reported a kind of unsymmetrical dendrimer, in which two different dendritic fragments were tethered together through the core.[8] Xu *et al.* prepared the dendritic–dendritic hybrid macromolecules through the consecutive cationic ring-opening polymerization of two AB_2 monomers, *i.e.* 3-ethyl-3-(hydroxymethyl) oxetane and glycidol.[9] The formed copolymers were expected to have a hyperbranched poly(3-ethyl-3-(hydroxymethyl)oxetane) core and a hyperbranched polyglycerol shell. Since the polarities of the core and the shell were similar, the amphiphilicity of this kind of copolymer was not expected to be obvious, which might be the reason that no further study on their guest encapsulation behavior was addressed.

Guest encapsulation is an area of considerable interest, due to its wide potential areas of application, including catalysis, reaction vessels, cosmetics, drug delivery and so forth.[10–12] Usually, the guest molecules are the desired active species,

[a]*Department of Chemistry, School of Sciences, Tianjin University, 300072 Tianjin, People's Republic of China. E-mail: chenyu@tju.edu.cn*
[b]*School of Chemistry and Materials Science, Ludong University, 264025 Yantai, Shandong Province, People's Republic of China*
[c]*Department of Polymer Materials Science and Engineering, School of Materials Science and Engineering, Tianjin University, 300072 Tianjin, People's Republic of China. E-mail: scjiang@tju.edu.cn*

† Electronic supplementary information (ESI) available: It includes the attempt to prepare the amphiphilic hyperbranched copolymers by another route, FTIR and ^{1}H NMR spectra of the polymers, tables showing the results of elemental analysis, DSC diagrams of the polymers, illustration of the encapsulation process, UV-vis spectra of dyes in water and chloroform, determination of the ε value of dye in chloroform, kinetic encapsulation, illustration of the core decrease upon increasing the degree of amidation and images of liquid–liquid encapsulation of different polymers for different guests. See DOI: 10.1039/c2sm25732g

whereas the hosts play the auxiliary roles, such as protecting or stabilizing the active guests. Under these circumstances, designing the hosts to have a high guest-encapsulation capacity is usually desired. To date, many kinds of amphiphilic core–shell type dendrimers,[13–18] hyperbranched polymers,[18–40] and multiarm star polymers with dendritic polymers as the core[41–58] have been addressed as unimolecular micelles being capable of encapsulating guest molecules in their dendritic core or in the inner shell of double-shell star polymers. It was found that amphiphilic dendritic polymers exhibited a superior performance in guest encapsulation to their corresponding linear analogues, due to their compact functional dendritic cores.[24–27] Until now, the shells of these reported amphiphilic dendritic polymers were usually formed by linear fragments, and amphiphilic dendritic polymers with branched shells were very scarce. Only very recently, Burakowska and Haag addressed a kind of amphiphilic core–shell type copolymer with a hyperbranched polyglycerol core, a long aliphatic hydrophobic inner shell, and a hyperbranched polyglycerol-based hydrophilic outer shell (ESI, Fig. S1A†).[49] This kind of polymer could be used as a unimolecular micelle to accommodate the nonpolar guest molecules into the linear inner shell, and the polymers with smaller outer shells showed a higher transport capacity for guests. Subsequently, Xia *et al.* reported another similar structure that had a dendritic polyester core, a linear poly(ε-caprolactone) inner shell and a hyperbranched polyglycerol outer shell (ESI, Fig. S1B†).[59] It was found that this polymer could also load the nonpolar guest molecules into the linear inner shell, and the number of loaded guests was dependent merely on the length of the linear segments, and not related to the dendritic core or the outer shell. The common property of both copolymers was that the dendritic core and the dendritic shell were separated by the functional linear segments, and the dendritic core was not responsible for guest accommodation. Moreover, the increase in the number of branching units in the outer shell harmed or had no influence on the guest encapsulation capacity of these nanocarriers.[49,59] Xu *et al.* synthesized mono-PEGylated and tri-PEGylated functionalized hyperbranched polyethylenimine (PEI), and the tri-PEGylated PEI could encapsulate more guest molecules than that of mono-PEGylated PEI (ESI, Fig. S1C†).[60] However, it was found that the guest molecules were distributed mainly in the shell, not in the functional PEI core.[50] Therefore, it is clear that until now the following points concerning the amphiphilic dendritic polymers have never been studied: (1) the synthesis of amphiphilic dendritic copolymers that have a dendritic core for the accommodation of guests and a dendritic shell for performance improvement; (2) comparative study of the influence of branched and linear shells on the performance of the functional dendritic core. Herein, we report the first real amphiphilic hyperbranched copolymers bearing a hyperbranched core and a dendritic shell, which could be used as nanocarriers to efficiently encapsulate hydrophilic guests. Moreover, compared with the corresponding nanocarriers with linear shells, we brought out firstly the opinion that the increase in shell branching promoted the guest encapsulation performance of the amphiphilic hyperbranched copolymer. This was contrary to the negative or no influence on the guest encapsulation capacity of the ever-reported multiarm star copolymers.[49,59]

Experimental

Materials

Hyperbranched polyethylenimine, PEI10K (Aldrich, $M_n = 10^4$ g mol^{-1}, $M_w/M_n = 2.5$) was dried under vacuum prior to use. Oxalyl dichloride (99%), pyridine (99%) and triethylamine (TEA, 99%) were purchased from Tianjin Kewei Chemical Company and purified by vacuum distillation before use. 2,2-Bis(hydroxymethyl)propionic acid (BHP, 99%) and 1,1′-carbonyldiimidazole (CDI, 97%) were purchased from Beijing Ouhe Technology Company and used directly. Benzoylated cellulose tubing (MWCO 1000) was purchased from Sigma and used directly. Dimethylformamide (DMF, A. R.) was refluxed with sodium and benzophenone before distillation. De-ionized water was double-distilled before use. Palmitic acid (A.R.) was purchased from Tianjin University Kewei Chemical Company and used directly. Congo Red (CR, $M_w = 696.7$ g mol^{-1}) was obtained from Tianjin Damao Reagent Factory. Methyl Orange (MO, $M_w = 327.3$ g mol^{-1}) was purchased from Tianjin Guangfu Fine Chemical Research Institute. Direct Blue 15 (DB, $M_w = 992.8$ g mol^{-1}) was purchased from Tokyo Chemical Industry Company. The syntheses of amphiphilic hyperbranched polymers with PEI as the core and linear palmitamide as the shell (PEI-C16) have been published elsewhere.[24,25]

Characterization

^{1}H and ^{13}C NMR spectra were recorded at 25 °C on a Varian INOVA 500 MHz spectrometer, operated at 500 MHz and 125 MHz, respectively. $CDCl_3$ was used as the solvent and the concentrations of the samples for the ^{1}H and ^{13}C NMR measurements are around 20 and 200 mg mL^{-1}, respectively. The chemical shifts (ppm) were referred to the internal calibration on the residual peak of the $CDCl_3$ solvent (^{1}H and ^{13}C NMR signals of $CDCl_3$ are 7.26 and 77.36 ppm, respectively). UV-vis spectra were obtained from a Purkinje General (China) T6 UV-vis Spectrophotometer. Elemental analysis was performed on an Elementar Vario ELCUBE. Differential scanning calorimetry (DSC) measurements were carried out on a Linkam Thermal Analysis System (DSC600) in the temperature range −20 to 120 °C at a heating rate of 10 °C min^{-1}. The melting temperature (T_m) was read off from the corresponding peak in the curve of the second heating process. Electrospray ionization/mass spectrometry (ESI-MS) was performed on a LCQ Advantage MAX. The FTIR spectrum was recorded on a Nicolet 5DXC FTIR spectrometer. The measurement was done using KBr pellets, and the scanning range was 4000–400 cm^{-1}.

Synthesis of BHP-based generation 1 dendron with two palmitate tails (D1-C16)

Under a nitrogen atmosphere, palmitoyl chloride (61.5 g, 0.224 mol) was added dropwise to the solution of BHP (12.0 g, 89.6 mmol) in 45 mL mixed solvents of DMF and pyridine (v/v = 1 : 2) at 25 °C with vigorous stirring. Subsequently, the reaction temperature was raised and kept at 50 °C for 5 h to finalize the reaction. After cooling to room temperature, the reaction mixture was dissolved in chloroform. This solution was washed twice with 6% diluted HCl aqueous solution, and then several times with

saturated NaCl aqueous solution until the pH value was close to 7. After the organic solution was dried with anhydrous $MgSO_4$, the volatiles were evaporated off under vacuum. The residue was recrystallized in acetone at around −18 °C at least three times to get the pure white product. Yield: 75%; FTIR: 1737 cm^{-1}(ν C=O of ester group), 1709 cm^{-1}(ν C=O of carboxylic acid group); ^{1}H-NMR ($CDCl_3$, δ ppm): 0.87 (t, 6H), 1.24 (br, 48H), 1.27 (s, 3H), 1.59 (m, 4H), 2.30 (t, 4H), 4.23 (m, 4H); ^{13}C-NMR ($CDCl_3$, δ ppm): 14.05, 17.73, 22.65, 24.85, 29.1–29.7, 31.9, 34.09, 46.16, 64.94, 173.23, 178.52; MS (ESI) *m/z*: $(M–H)^-$, 609.21 (calcd 609.94). Elemental analysis: 73.01% C, 11.25% H, 15.74% O (calcd 72.74% C, 11.55% H, 15.71% O); T_m: 59.8 °C.

Acyl chlorination of D1-C16 (Cl-D1-C16)

Oxalyl chloride (49.9 g, 0.392 mol) was added dropwise to D1-C16 (60.0 g, 98.2 mmol) in 250 mL anhydrous dichloromethane with vigorous stirring. After six hours, the volatiles were removed under reduced pressure. The obtained product was dried for 24 h in vacuum. Yield: 99%. ^{1}H NMR ($CDCl_3$, δ ppm): 0.87 (t, 6H); 1.24 (br, 48H), 1.36 (s, 3H), 1.59 (m, 4H), 2.31 (t, 4H), 4.27 (s, 4H).

Synthesis of BHP-based generation 2 dendron with four palmitate tails (D2-C16)

Under a nitrogen atmosphere, Cl-D1-C16 (20.5 g, 32.5 mmol) was added dropwise to the solution of BHP (1.45 g, 10.8 mmol) in 80 mL mixed solvents of DMF and pyridine (v/v = 1 : 2) at 25 °C with vigorous stirring. Subsequently, the reaction temperature was raised and kept at 50 °C for 5 h to finalize the reaction. After cooling to room temperature, the reaction mixture was dissolved in chloroform. This solution was washed twice with 6% diluted HCl aqueous solution, and then several times with saturated NaCl aqueous solution until the pH value was close to 7. After the organic solution was dried with anhydrous $MgSO_4$, the volatiles were evaporated off under vacuum. The residue was recrystallized in methanol at around −18 °C at least three times. Much pure product could be obtained by dialysis against chloroform using a benzoylated cellulose membrane (MWCO 1000 g mol^{-1}) for 3 days. Yield: 40%; FTIR: 1740 cm^{-1} (ν C=O of ester group); ^{1}H-NMR ($CDCl_3$, δ ppm): 0.87 (t, 12H), 1.24 (br, 105H), 1.57 (m, 8H), 2.28 (t, 8H), 4.15–4.27 (m, 12H); ^{13}C-NMR ($CDCl_3$, δ ppm): 14.04, 17.72, 22.63, 24.83, 29.11–29.65, 31.89, 34.01, 46.31, 46.42, 64.95, 65.77, 173.22, 175.72, 177.21; MS (ESI) *m/z*: $(M–H)^-$, 1318.4 (calcd 1319.0). Elemental analysis: 71.39% C, 11.83% H, 16.78% O (calcd 71.88% C, 11.15% H, 16.97% O); T_m: 24.7 °C.

Acyl chlorination of D2-C16 (Cl-D2-C16)

Oxalyl chloride (0.98 g, 7.72 mmol) was added dropwise to D2-C16 (2.55 g, 1.93 mmol) in 25 mL anhydrous dichloromethane with vigorous stirring. After six hours, the volatiles were removed under reduced pressure. The obtained product was dried for 24 h in vacuum. Yield: 99%. ^{1}H NMR ($CDCl_3$, δ ppm): 0.87 (t, 6H), 1.24 (br, 102H), 1.38 (br, 3H), 1.57 (m, 8H), 2.28 (t, 8H), 4.15–4.27 (m, 12H).

Synthesis of polymers with PEI as the core and D1-C16 or D2-C16 as the shell

This is exemplified for the polymer PD1-3 in Table 1. Under a nitrogen atmosphere, Cl-D1-C16 (4.3 g, 6.8 mmol) was added dropwise to the solution of PEI (0.40 g) and TEA (0.76 g, 7.4 mmol) in 80 mL anhydrous chloroform at 0–5 °C with vigorous stirring. Then, the mixture was stirred for another 6 h at room temperature. After cooling to room temperature, the reaction mixture was washed twice with saturated NaCl aqueous solution. Afterwards, the organic phase was concentrated, and then precipitated from excess acetone. The precipitate was collected through centrifugation, and dried at room temperature under vacuum overnight. The obtained product was in the form of a yellowish power; yield: 90%.

Measurement of molar extinction coefficients (ε) of dyes in water and chloroform

The determination of the ε value in water: a series of different concentrations of dye in water was prepared and measured by UV-vis spectrophotometry. The maximal absorbance (Abs) *vs.* dye concentration was plotted, and a linear relationship through the origin was obtained at an absorbance below 2. According to the Lambert–Beer law (Abs = εcl, c is the dye concentration, l is the thickness of the cuvette, which is 1 cm), the ε value could be read off from the slope. The ε values of MO, CR and DB in water were measured as 2.28×10^4 (465 nm), 3.91×10^4 (497 nm) and 1.53×10^4 (592 nm) L mol^{-1} cm^{-1}, respectively.

The determination of the ε value in chloroform: the aqueous solution of the dye of known concentration was mixed with the same volume of polymer in chloroform (0.55–0.0142 mg mL^{-1}). The solution was shaken for 10 minutes and equilibrated at room temperature in a dark chamber overnight. The concentrations of the dye and polymer were adjusted to make sure that the water phase was finally colorless. In order to ensure that all the dyes in water could be transferred into the chloroform phase, the final water–chloroform interface should be clear and clean, and no precipitate should be detected visibly. It should be noted here that only a polymer with a branched shell could fully satisfy the above-mentioned phenomenon. Then, the chloroform solution of the polymer–dye complex was diluted into different dye concentrations, and measured by UV-vis spectrophotometry. The maximal absorbance (Abs) *vs.* dye concentration in chloroform was plotted, and a linear relationship across the origin of the coordinates was obtained at an absorbance below 2. According to the Lambert–Beer law, the ε value was read off from the slope. The ε values of MO, CR and DB in chloroform were measured to be 2.87×10^4 (427 nm), 3.81×10^4 (506 nm) and 1.43×10^4 (601 nm) L mol^{-1} cm^{-1}, respectively.

Methodology for dye extraction in phase transfer processes

The chloroform solution of the polymer (1×10^{-7} to 2×10^{-6} M) was mixed with the same volume of aqueous solution of the dye. The solution was shaken for 10 minutes and equilibrated at room temperature in a dark chamber for 2–4 days. The dye concentration was adjusted to make sure that only part of the dye in the water was transferred into the $CHCl_3$ phase. The chloroform phase was measured by UV-vis spectrophotometry. According to

Table 1 Structural parameters of the obtained amphiphilic hyperbranched polymers and their thermal properties from DSC

		^{1}H NMR analysis[c]			Elemental analysis			DSC analysis	
Polymer	Shell	DA[a]	DS_{C16}[b]	$M_n/10^4$	DA	DS_{C16}	$M_n/10^4$	T_m/°C	ΔH_m/J^{-1} g^{-1}
PD2-1	D2-C16	0.27	1.08	9.2	0.27	1.08	9.2	18.4	24.1
PD1-1	D1-C16	0.27	0.54	4.7	0.28	0.56	4.9	—	—
PD1-2	D1-C16	0.41	0.82	6.7	0.39	0.78	6.4	27.6	23.4
PD1-3	D1-C16	0.54	1.08	8.4	0.46	0.92	7.3	32.0	35.6
PL-1	C16	0.27	0.27	2.5	0.31	0.31	2.7	59.7	40.0
PL-2	C16	0.54	0.54	4.0	0.47	0.47	3.6	63.5	42.8
PL-3	C16	0.73	0.73	5.0	0.67	0.67	4.7	65.7	47.5

[a] DA represents degree of amidation relative to the total amino groups of PEI. [b] DS_{C16} represents degree of substitution of the C16 chain relative to the total amino groups of PEI. [c] DA (PEI-C16) = $(I_a/3)/(I_{PEI}/4) = 4I_a/(3I_{PEI}) = DS_{C16}$; DA (PEI-D1-C16) = $(I_a/3)/2/(I_{PEI}/4) = 2I_a/(3I_{PEI}) = 0.5DS_{C16}$; DA (PEI-D2-C16) = $(I_a/3)/4/(I_{PEI}/4) = I_a/(3I_{PEI}) = 0.25DS_{C16}$; I_a is the integral of methyl protons of the C16 chain in ^{1}H NMR; I_{PEI} is the integral of ethylene protons of PEI moieties in ^{1}H NMR (ESI, Fig. S3†).

the Lambert–Beer law and the obtained ε value of dye in chloroform, the number of dye molecules encapsulated by the polymer could therefore be obtained.

Results and discussion

Until now many amphiphilic hyperbranched polymers showing unimolecular micellar properties have been reported.[18–40] Among those polymers, the unimolecular micellar nanocarriers derived from amidation of the hyperbranched PEI with 1,1′-carbonyldiimidazole (CDI) activated palmitic acid or palmitoyl chloride (PEI-C16) exhibited a very high encapsulation efficiency for hydrophilic anionic dyes.[24,25] For instance, with respect to the large hydrophilic Congo Red (CR) guest, other nanocarriers based on PEI or other hyperbranched polymers could only encapsulate around one or fewer than one CR guest per nanocarrier,[21,35] whereas one PEI-C16 nanocarrier could accommodate more than 10 CRs using its amidated PEI core.[24] Therefore, for accuracy, PEI-C16 is a suitable standard for the study of the influence of shell morphology on the performance of the amphiphilic hyperbranched copolymers. In this article, the targeted amphiphilic copolymers have a hydrophilic dendritic core formed by amidated PEI, and a hydrophobic dendritic shell formed by branching units and long hydrophobic chains, as shown in Scheme 1.

The employed PEI contains primary, secondary and tertiary amine functional groups, and their molar ratio is about 33 : 40 : 27.[55] The degree of branching is around 60%. BHP is used as the building block for the branching units in the shell. Palmitoyl chloride is employed to form the long hydrophobic chain. Two routes have been adopted for the introduction of branching units into the desired polymers. One is the divergent method (ESI, Scheme S1†). Firstly, PEI reacted with acetonide-protected BHP under various conditions, including the direct amidation reaction at high temperature, CDI activated acetonide-protected BHP and acetonide-protected BHP anhydride. However, it was found that it was difficult for all the reactive primary and secondary amines of PEI to react with BHP, and the maximum degree of amidation (DA) was only around 50%. Since both the hydroxyl groups of the BHP units and the residual amino groups of PEI could react with palmitic acid and its derivatives, it was difficult to precisely control the long aliphatic chains such that they attached only onto the branched BHP units, and not onto the residual amines of PEI. Subsequently, a convergent method was adopted (Scheme 1). First, BHP reacted with palmitoyl chloride to form the generation 1 dendron (D1-C16), composed of two long aliphatic chains and one carboxylic acid group. Then, one BHP was coupled with two D1-C16 dendrons to form the generation 2 dendron (D2-C16), with four aliphatic chains and one carboxylic acid group. The carboxylic acid groups of D1-C16 and D2-C16 were activated through the acyl chlorination reaction, and were then coupled with PEI through the amidation reaction. This resulted in polymers with PEI as the core and branched D1-C16 and D2-C16 as the shell, and they were abbreviated as PEI-D1-C16 and PEI-D2-C16, respectively.

The obtained PEI-D1-C16 and PEI-D2-C16 polymers were characterized by FTIR (ESI, Fig. S2†). By comparison with the FTIR spectrum of PEI-C16, the strong absorption at 1647 cm^{-1} in the FTIR spectra of the resulting PEI-D1-C16 and PEI-D2-C16 copolymers can be assigned as the characteristic C=O stretching bond frequency of the amide groups, indicating the successful transformation of the amine groups of PEI into amide groups by reacting with D1-C16 or D2-C16. Compared with the FTIR spectra of D1-C16 or D2-C16, the strong absorption at 1744 cm^{-1}, characteristic of the C=O stretching bond frequency of ester groups, is another indication of the successful introduction of D1-C16 or D2-C16 moieties onto PEI.

The resulting polymers and their precursors were also characterized by ^{1}H NMR (ESI, Fig. S3†). The signals of the obtained PEI-D1-C16 and PEI-D2-C16 copolymers are assigned by comparison with the ^{1}H NMR spectra of D1-C16, D2-C16 and PEI-C16. All the signals coming from the PEI, D1-C16 and D2-C16 moieties can be found. Moreover, the new broad multiple signals between 3.0 and 3.9 ppm in Fig. S3D and E† are the methylene protons of the PEI moiety adjacent to the amide groups, which is strong evidence of the successful amidation reaction between the amino groups of PEI and D1-C16 or D2-C16. From the integral (I) ratio of the signals coming from the methyl protons (signal a at around 0.86 ppm) of the C16 chains with the PEI scaffold (broad signals between 2.3 and 3.8 ppm) in the ^{1}H NMR spectra, the average degree of amidation (DA) and the degree of substitution of the C16 (DS_{C16}) chain relative to the total amino groups of PEI can be calculated. Table 1 shows the

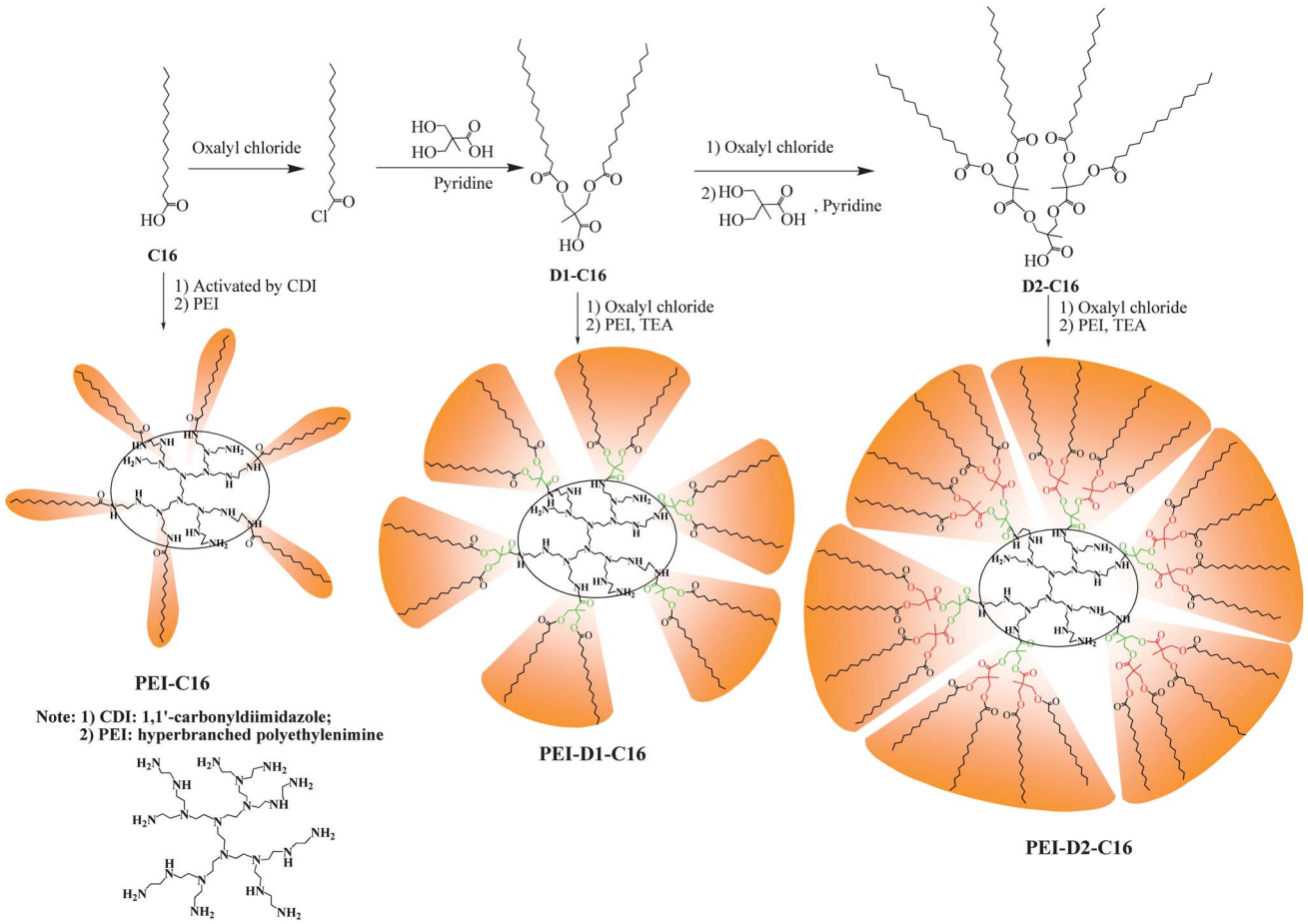

Scheme 1 Syntheses of amphiphilic copolymers with a hydrophilic amidated PEI core and a hydrophobic linear or branched shell.

structural information for the obtained copolymers deduced from NMR, including DA, DS_{C16}, and molecular weight. For comparison, elemental analysis was carried out for all the copolymers (ESI, Table S1†) and the same structural parameters were also calculated and listed in Table 1. It is clear that the structural parameters calculated from both analytical methods are similar and that the difference is within 15%.

In order to study the effect of shell branching on the properties of the amphiphilic hyperbranched copolymers, we prepared three series of samples as listed in Table 1: (1) three PEI-C16 polymers with different DA values whose shells are composed of linear C16 chains (PL-1, PL-2 and PL-3); (2) three PEI-D1-C16 polymers with different DA values whose shells are composed of branched D1-C16 chains (PD1-1, PD1-2 and PD1-3); (3) one PEI-D2-C16 polymer whose shell consists of branched D2-C16 chains (PD2-1). As for the PEI-D2-C16 polymer, the DA value of the obtained sample is *ca.* 27%. Attempts to further increase the DA value of this series of polymers failed. With respect to PEI-D1-C16 polymers, the maximal DA value that could be reached was around 60%, whereas the DA value of PEI-C16 could be controlled intentionally. This is a normal phenomenon, since branched D2-C16 and D1-C16 are more bulky than the linear C16, which leads to a serious steric hindrance effect during the amidation reaction.

The thermal properties of these amphiphilic hyperbranched copolymers were measured by DSC (ESI, Fig. S4†). Hyperbranched PEI in general does not crystallize. However, attachment of linear C16 induces crystallization. The melting temperature (T_m) and melting enthalpy (ΔH_m) increase with the increase of DS_{C16} (see PL-1, PL-2 and PL-3 in Table 1). Crystallization can also be induced by the attachment of branched D1-C16 and D2-C16 only when the DS_{C16} value is high enough (Table 1). For instance, as for PEI-D1-C16 with $DS_{C16} = 0.54$ (PD1-1), no obvious crystallization can be detected in the DSC diagram. The increase of the DS_{C16} value to 0.82 or more leads to the appearance of a melting peak. Comparing the samples with similar DS_{C16} values in Table 1 (comparing PD2-1 with PD1-3; PD1-1 with PL-2), it can be seen that the samples with less branched shells have higher T_m and ΔH_m. This indicates that the introduction of branching sites in the shell can pronouncedly reduce the crystallinity of the amphiphilic copolymers.

The obtained polymers have a distinct core–shell structure, since their amidated PEI part is very hydrophilic compared with their aliphatic amide moieties, which have high hydrophobic olefin contents. Thus, the obtained amphiphilic hyperbranched copolymers are expected to display an inverted micellar behavior, *i.e.* the hydrophobic aliphatic amide moieties forming the shell domain help to stabilize the interface between the hydrophilic amidated PEI core and the external apolar solvent, and the hydrophilic amidated PEI core can supply a microenvironment for the accommodation of hydrophilic guest molecules

due to their similar polarities, leading to the hydrophilic guest molecules being able to dissolve in their poor solvents. Therefore, the guest encapsulation behaviors of these amphiphilic hyperbranched copolymers with linear and branched shells as nanocarriers were compared. First, the typical water-soluble anionic dye guests, Methyl Orange (MO), Congo Red (CR) and Direct Blue 15 (DB), having different sizes and numbers of functional groups (Chart 1), were used as a probe. The normal liquid–liquid encapsulation protocol was adopted (ESI, Fig. S5†): the same volume solutions of dye in water and the polymers in $CHCl_3$ were taken, mixed and shaken. The evidence that dyes were encapsulated by polymers was that after phase separation, the colorless organic phase became colored and the concentration of dyes in the water phase decreased, which could be confirmed from the decrease in UV-vis absorbance of the dyes in the water phase. Moreover, the maximum absorption band displayed a hypsochromic shift for MO, and a bathochromic shift for CR and DB in the chloroform phase compared with their maximum absorption in water (ESI, Fig. S6†), pointing to the creation of a new environment for the water-soluble guests in the amphiphilic hyperbranched copolymers.

For quantitative calculation of the number of dyes loaded by the nanocarrier from the UV-vis spectra, the molar extinction coefficient (ε) values of the dyes encapsulated by the nanocarrier in chloroform were measured. First, we studied the effect of the number of loaded dyes per nanocarrier on the ε values of MO, CR and DB in chloroform. It was found that the number of dyes encapsulated by each nanocarrier had nearly no influence on the ε values of MO, CR and DB in chloroform (ESI, Fig. S7†). The obtained ε values of MO, CR and DB in chloroform were measured to be 2.87×10^4 (427 nm), 3.81×10^4 (506 nm) and 1.43×10^4 (601 nm) L mol^{-1} cm^{-1}, respectively. These values were different from the corresponding 2.28×10^4 (465 nm), 3.91×10^4 (497 nm) and 1.53×10^4 (592 nm) L mol^{-1} cm^{-1} of MO, CR and DB in water. For the accurate measurement of the guest encapsulation capacity of the obtained nanocarriers, the following factors were considered. First, the time required for the partition equilibrium of guests in the two phases was studied (ESI, Fig. S8†). It was found that the required time differed from tens to hundreds of minutes for different polymer systems, but equilibrium could be reached at most one day later. Therefore, for all the encapsulation experiments, the two phase mixtures were equilibrated at room temperature for at least one day before the UV-vis spectrometry measurement.

Second, the effect of nanocarrier concentration on their encapsulation capacity was also studied. From Fig. 1A it can seen that the amount of dye transferred to the organic phase increases linearly when the nanocarrier concentration is below 1×10^{-6} M and the intercept is 0, which implies that all the nanocarriers exist as unimolecular micelles within this low polymer-concentration range.[37] From Fig. 1B it is clear that the encapsulation capacities of all the nanocarriers studied here are less dependent on their concentrations. In order to assure that all the nanocarriers exist as unimolecular micelles during the guest encapsulation process, the concentration of the nanocarriers is fixed at around 5×10^{-7} M in the following experiments.

Third, with respect to the effect of the dye concentration on the encapsulation capacity of the nanocarriers, it is obvious that a higher concentration of dye results in a pronounced higher guest loading at the beginning, but the increase becomes not so significant when a more concentrated dye solution is used (Fig. 2). Hence, for the effective comparison of different

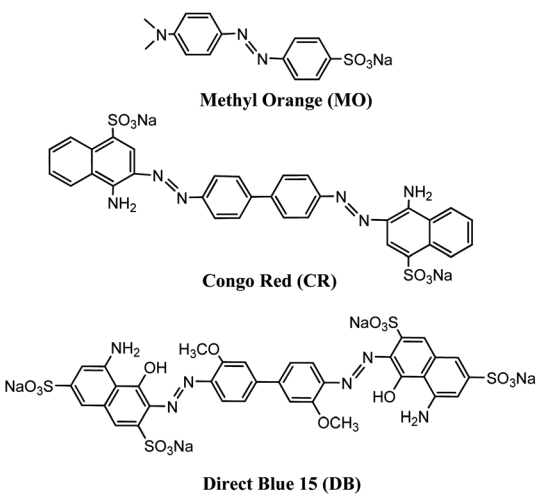

Chart 1 The molecular structure of MO, CR and DB.

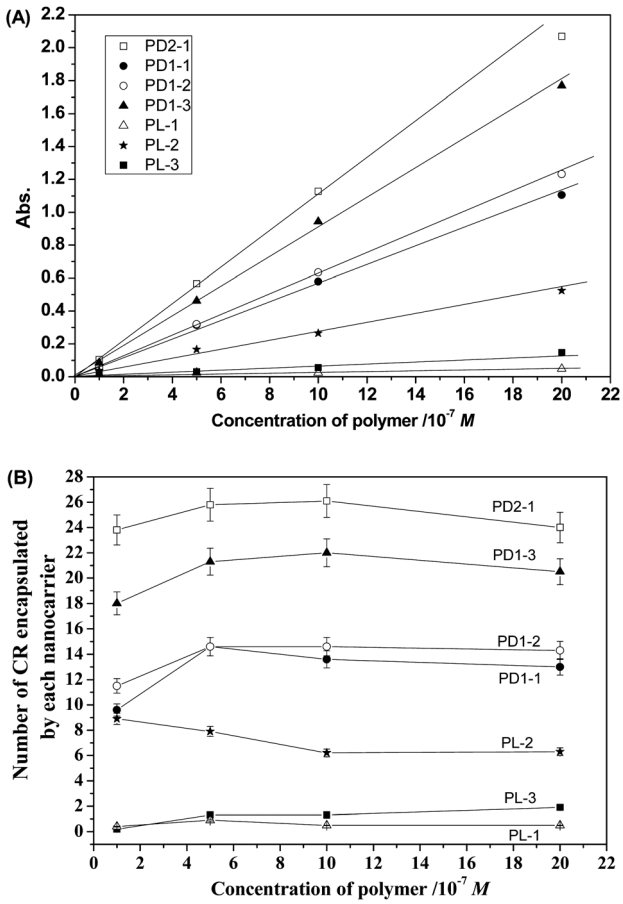

Fig. 1 The effect of polymer concentration on (A) the absorbance intensity of CR at 506 nm in chloroform and (B) the encapsulation capacity of the nanocarrier (initial concentration of CR in water is 0.30 mg mL^{-1}).

nanocarriers, the concentrations of dyes used are high enough to make sure that the encapsulation capacity of different nanocarriers is close to the maximum value. Moreover, for the comparative study of the influence of the dyes' structure on the encapsulation capacity of the nanocarriers, the molar concentrations of all the dyes are kept the same.

Fig. 3A shows the average number of dye molecules encapsulated by each nanocarrier. For accuracy of the data, each encapsulation experiment was repeated at least twice. We found that the data could be repeated very well and the error was within 5%. When the type of shell is fixed, the influence of DA alteration on the encapsulation capacity of the nanocarriers for all the three guests has the same trend. For example, with respect to the nanocarriers with D1-C16 as the shell, the ordering of their encapsulation capacity for all three guests is PD1-3 > PD1-2 > PD1-1. As for the nanocarriers with linear C16 as the shell, the ordering is PL-2 > PL-3 > PL-1. Furthermore, when the size of the polar core is similar, in other words the DA value is similar, the nanocarriers with more branched shells show a higher encapsulation capacity (PD2-1 > PD1-1 > PL-1; PD1-3 > PL-2). Moreover, from Fig. 3A it can be seen that the nanocarriers with branched shells can encapsulate dyes much more than those with linear shells. For instance, among the three nanocarriers with linear shells, PL-2 is the best. The average numbers of MO, CR and DB molecules loaded by one PL-2 are about 27, 8 and 16, respectively, whereas the average numbers of MO, CR and DB molecules loaded by one PD1-3 are about 51, 21 and 60, respectively. Why do the nanocarriers with branched shells show such significant enhancement of the guest encapsulation performance? We tentatively explained this phenomenon as follows: first, it should make sure where the polar guests could be accommodated in the nanocarrier. From the previous study on the inverted 'unimolecular' micelles with amidated PEI as the hydrophilic core, it was known that the hydrophilic guests were accommodated in the hydrophilic core.[24,25] The first reason is due to their similar polarity. The second reason is that the guest molecules can strongly interact with the amidated PEI core through both hydrogen-bonding and electrostatic interactions. The third reason is that increasing the size and polarity of the amidated PEI core are two effective ways to pronouncedly

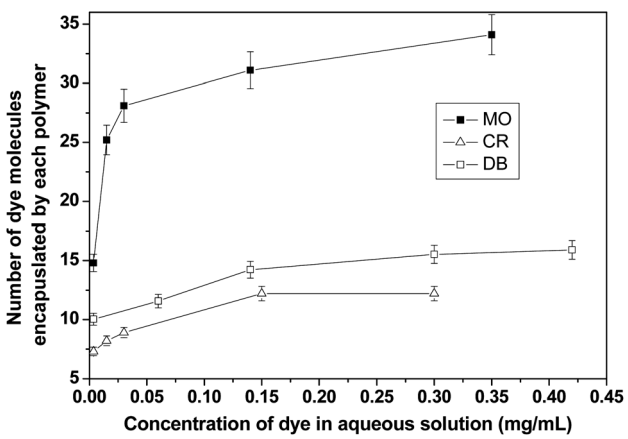

Fig. 2 The effect of initial dye concentration on the encapsulation capacity of the nanocarrier (PL-2 was used, and the polymer concentration is around 5×10^{-7} M).

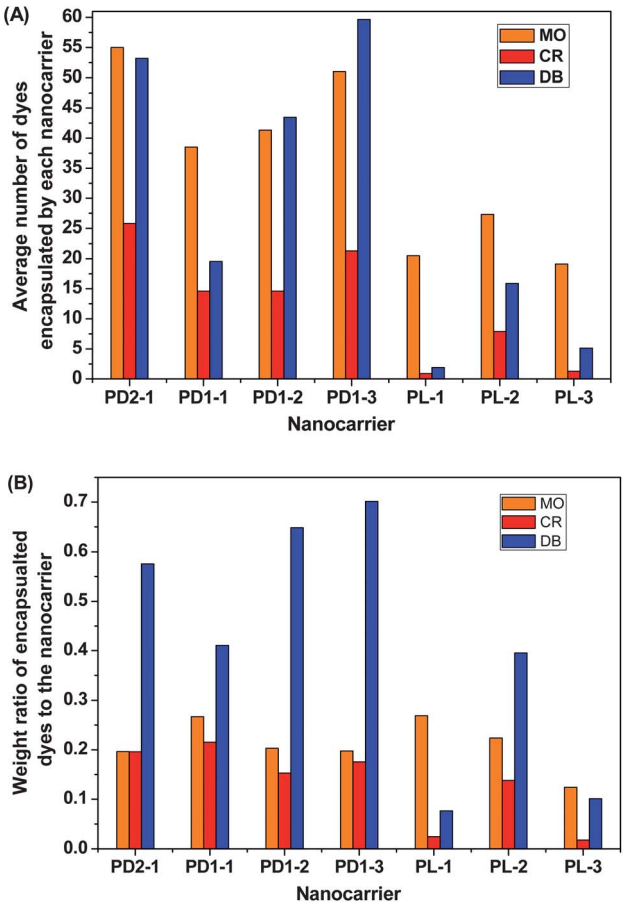

Fig. 3 (A) The average number of dyes encapsulated by each nanocarrier; (B) the weight ratio of encapsulated dyes to the nanocarrier (polymer concentration is around 5×10^{-7} M, initial concentration of MO, CR and DB is 0.14, 0.30 and 0.43 mg mL^{-1}, respectively, [MO] = [CR] = [DB] = 4.3×10^{-4} M).

enhance the hydrophilic guest encapsulation capacity of the nanocarriers. The only difference between the nanocarriers with linear and branched shells studied here lies in the middle dendritic layer consisting of a large number of ester groups, which should be the key point for the superior performance of nanocarriers with a branched shell. Now the question arises as to how this middle layer contributes to the significant enhancement of the guest encapsulation capacity of the nanocarriers. Is it because the large number of ester groups can also interact with the hydrophilic guests through the weak noncovalent interaction? Or is it due to the dendritic structure, which helps the amidated PEI to accommodate more guests? Previously, we have prepared a series of core–shell type multiarm star polymers with PEI as the core and poly(ε-caprolactone) as the shell.[55–57] It was found that the significant increase in the hydrophobic polyester arm length could only enhance the guest encapsulation capacity a little, and the increase in the guest encapsulation capacity could be ascribed to the increase of hydrophobic moieties, not the existence of ester groups. Thus, it could be deduced that the pronounced increase in encapsulation performance of the nanocarriers with branched shells was not due to the introduction of the large number of ester groups, and the possible weak noncovalent interaction between ester groups and

hydrophilic guests contributed to the high encapsulation performance only a little or not at all. Hence, it implies that it is the introduction of the dendritic structure in the middle layer that favors the pronounced enhancement of the encapsulation performance. Why does the dendritic structure favor a high encapsulation capacity? One plausible reason might be that the dendritic layer can make the hydrophobic shell denser as shown in Scheme 1, while keeping the size of the hydrophilic core the same. The denser shell will render the hydrophilic core more rigid and slow its dynamic motion more. This might lead to the dynamic cavity for the accommodation of guests having a longer lifetime. Thus, more guests can stay in the dynamic cavities of the nanocarriers with denser shells. From the above discussion, it is clear that a larger hydrophilic core and denser hydrophobic shell are two important factors for the higher encapsulation capacity of the nanocarriers. With respect to nanocarriers with linear shells, the increase in hydrophobic moieties means that the size of the hydrophilic core size will decrease (ESI, Fig. S9†). The interplay between these two factors decides that a maximal encapsulation capacity can be reached when the nanocarrier has enough hydrophobic moieties. However, the further increase in hydrophobic moieties cannot compensate for the decrease in the hydrophilic core size, resulting in a decrease in encapsulation capacity. This is a normal phenomenon for the nanocarriers with linear shells.[21] As for the nanocarriers with branched shells, the increase in hydrophobic moieties can compensate for the decrease in the hydrophilic core size since the increase in hydrophobic moieties is 2 or 4-fold higher than that of the nanocarriers with linear shells.

The encapsulation behaviors of these nanocarriers for different guests were also compared. All the guests including MO, CR and DB are water-soluble and rod-like (Chart 1). Among these guests, DB is the most polar one, and bears 4 very polar sulfonates, two middle polar phenols and two middle polar anilines. Moreover, it is also the biggest, whereas MO is the smallest and the least polar one, since it only contains one very polar sulfonate and one less polar tertiary amine group. As for CR, its size is in the middle and its polarity is also in the middle, since it contains two very polar sulfonates and two middle polar anilines. First, let us consider the nanocarriers with branched shells. The quantities of MO and DB molecules encapsulated by most of these nanocarriers are similar, while obviously being higher than CR (Fig. 3A). Since the size of DB is nearly three times larger than that of MO, the similarly loaded quantities of MO and DB by the nanocarriers with branched shells mean that DB can be encapsulated by the nanocarriers with branched shells more efficiently due to its very high polarity. Here the size of the guest is not the deciding factor. This can also be seen clearly from the data of the weight ratio of the encapsulated guests to the nanocarrier (Fig. 3B), where the weight ratio of the encapsulated DB guests to the nanocarrier is much higher than the weight ratio of the encapsulated MO guests to the nanocarrier. As for CR, its size is more than two times larger than MO, whereas the nanocarriers with branched shells encapsulate MO more than two times but less than three times as more as CR (Fig. 3A). As far as the weight ratio of the encapsulated guests to the nanocarrier is concerned, it is similar for MO and CR (Fig. 3B). The above results indicate that when the polarity difference of the guests is not big enough, the encapsulation capacity of the nanocarriers with branched shells has a strong relationship with the size of the guest. As for the nanocarriers with linear shells, their encapsulation efficiencies (the weight ratio of encapsulated guests to the nanocarrier) for MO are not very different from those of the nanocarriers with branched shells (Fig. 3B). However, the encapsulation efficiencies of the nanocarriers with linear shells, especially PL-1 and PL-3, are not as good as those of the nanocarriers with branched shells, for CR and DB. Why do the nanocarriers with branched and linear shells show such different encapsulation behaviors for these three dyes? In the encapsulation experiments of the nanocarriers with branched shells, no matter what guests were used, the final oil–water interface was all clean and clear. However, in the encapsulation experiments of nanocarriers with linear shells, only when MO was used was the final oil–water interface clean and clear. With respect to CR and DB, the final oil–water interface usually contained some precipitates with the corresponding dye color (ESI, Fig. S10†). This implies that some CR and DB molecules precipitate during the encapsulation process, which might be the reason why the nanocarriers with linear shells cannot encapsulate CR and DB as efficiently as those with branched shells. The different behaviors of these nanocarriers for MO, CR and DB were explained tentatively as follows: as far as the guests are concerned, MO has only one functional sulfonate group, thus it can only interact with one nanocarrier. CR and DB are bigger and have more than one sulfonate group, thus it is possible for them to simultaneously interact with more than one nanocarrier to form the insoluble nanocarrier–guest network. As far as the nanocarriers are concerned, the ones with linear shells can conveniently transform and expose their core due to their flexibility. This increases the chance that multifunctional guests can interact with several nanocarriers to form the network. As for the nanocarriers with branched shells, the dendritic middle layer makes the core more rigid and it cannot transform so conveniently as those of the nanocarriers with linear shells. Thus, the chance that one multifunctional guest interacts with several nanocarriers is minor due to the steric hindrance effect.

The encapsulation capacity of the novel amphiphilic hyperbranched copolymers was also compared with other similar systems bearing the PEI core and the hydrophilic shell (Table S2†).[18,21,23,24,56] Most of the encapsulation systems only supplied data for the molar ratio of encapsulated guests to the nanocarrier. From the limited data comparison, it can be deduced that the novel encapsulation systems shown in this paper have a moderate guest-encapsulation capacity. Since the aim of this paper is to study the effect of shell morphology on the encapsulation capacity of nanocarriers, we have not attempted to change other parameters to maximize the encapsulation capacity of these novel nanocarriers. In subsequent work, we shall try to enhance the encapsulation capacity of these nanocarriers through tuning other parameters.

Conclusions

Amphiphilic hyperbranched copolymers bearing a hyperbranched core and a dendritic shell were successfully prepared through the amidation reaction between PEI and D1-C16 or D2-C16. The existence of the branching units in the shell pronouncedly reduced the crystallinity of the amphiphilic

hyperbranched copolymers. The copolymers with less branched shells had higher values of T_m and ΔH_m.

These amphiphilic hyperbranched copolymers could be used as nanocarriers to efficiently accommodate the hydrophilic guests, including MO, CR and DB, into the hydrophilic amidated PEI core. The dendritic structure of the shell of these new nanocarriers contributed pronouncedly to their superior encapsulation performance over the nanocarriers with linear shells. As far as the weight ratio of the encapsulated guests to the nanocarriers was concerned, the nanocarriers with branched and linear shells could be tuned to have a similar encapsulation capacity for the small MO with a mono-sulfonate group. However, the nanocarriers with branched shells could be modulated to have a much superior encapsulation capacity to the nanocarriers with linear shells, for the larger CR and DB with multi-sulfonate groups.

From the experimental results, it can be concluded that for the effective enhancement of the guest encapsulation performance of amphiphilic dendritic polymers, besides the well-known methods of increasing the size and polarity of the core, the introduction of branching units in the shell is also an effective method.

Acknowledgements

The authors are grateful for the financial support from the Program for New Century Excellent Talents in University, and the National Natural Science Foundation of China (20974077, 21074088).

Notes and references

1 G. R. Newkome, C. N. Moorefield and F. Vögtle, *Dendritic Molecules: Concepts, Synthesis, Perspectives*, VCH, Weinheim, 2001.
2 D. Astruc, E. Boisselier and C. Ornelas, *Chem. Rev.*, 2010, **110**, 1857–1959.
3 C. Gao and D. Yan, *Prog. Polym. Sci.*, 2004, **29**, 183–275.
4 H. Frauenrath, *Prog. Polym. Sci.*, 2005, **30**, 325–384.
5 S. J. Teertstra and M. Gauthier, *Prog. Polym. Sci.*, 2004, **29**, 277–327.
6 F. Wurm and H. Frey, *Prog. Polym. Sci.*, 2011, **36**, 1–52.
7 D. Wilms, S.-E. Stiriba and H. Frey, *Acc. Chem. Res.*, 2010, **43**, 129–141.
8 K. L. Wooley, C. J. Hawker and J. M. J. Fréchet, *J. Am. Chem. Soc.*, 1993, **115**, 11496.
9 Y. Xu, C. Gao, H. Kong, D. Yan, P. Luo, W. Li and Y. Mai, *Macromolecules*, 2004, **37**, 6264–6267.
10 G. Barrat, *Cell. Mol. Life Sci.*, 2003, **60**, 21–37.
11 J. L. Chávez, J. L. Wong, A. V. Jovanovic, E. K. Sinner and R. S. Duran, *IEE Proc.: Nanobiotechnol.*, 2005, **152**, 73–84.
12 M. Irfan and M. Seiler, *Ind. Eng. Chem. Res.*, 2010, **49**, 1169–1196.
13 C. J. Hawker, K. L. Wooley and J. M. J. Fréchet, *J. Chem. Soc., Perkin Trans. 1*, 1993, 1287–1297.
14 K. R. Copidas, A. R. Leheny, G. Caminati, N. J. Turro and D. A. Tomalia, *J. Am. Chem. Soc.*, 1991, **113**, 1335–1342.
15 S. Stevelmans, J. C. M. van Hest, J. F. G. A. Jansen, D. A. F. J. van Boxtel, E. M. M. de Brabander-van den Berg and E. W. Meijer, *J. Am. Chem. Soc.*, 1996, **118**, 7398–7399.
16 M. W. P. L. Baars, P. E. Froehling and E. W. Meijer, *Chem. Commun.*, 1997, 1959–1960.
17 A. I. Cooper, J. D. Londono, G. Wignall, J. B. McClain, E. T. Samulski, J. S. Lin, A. Dobrynin, M. Rubinstein, A. L. C. Burke, J. M. J. Fréchet and J. M. DeSimone, *Nature*, 1997, **389**, 368–371.
18 A. Garcia-Bernabé, M. Krämer, B. Olah and R. Haag, *Chem.–Eur. J.*, 2004, **10**, 2822–2830.
19 A. R. Esker, L.-H. Zhang, C. E. Olsen, K. No and H. Yu, *Langmuir*, 1999, **15**, 1716–1724.
20 R. K. Kainthan and D. E. Brooks, *Bioconjugate Chem.*, 2008, **19**, 2231–2238.
21 M. Krämer, J.-F. Stumbé, H. Türk, S. Krause, A. Komp, L. Delineau, S. Prokhorova, H. Kautz and R. Haag, *Angew. Chem., Int. Ed.*, 2002, **41**, 4252–4256.
22 Y. H. Kim and O. W. Webster, *J. Am. Chem. Soc.*, 1990, **112**, 4592–4593.
23 D. Wan, H. Pu and X. Cai, *Macromolecules*, 2008, **41**, 7787–7789.
24 Y. Chen, Z. Shen, L. Pastor-Pérez, H. Frey and S.-E. Stiriba, *Macromolecules*, 2005, **38**, 227–229.
25 H. Liu, Y. Chen, D. Zhu, Z. Shen and S.-E. Stiriba, *React. Funct. Polym.*, 2007, **67**, 383–395.
26 S.-E. Stiriba, H. Kautz and H. Frey, *J. Am. Chem. Soc.*, 2002, **124**, 9698–9699.
27 K. R. Kumar and D. E. Brooks, *Macromol. Rapid Commun.*, 2005, **26**, 155–159.
28 D. Wan, J. Yuan and H. Pu, *Macromolecules*, 2009, **42**, 1533–1540.
29 D. Wan, G. Wang, H. Pu and M. Jin, *Macromolecules*, 2009, **42**, 6448–6456.
30 J. Zou, Y. Zhao and W. Shi, *J. Phys. Chem. B*, 2006, **110**, 2638–2642.
31 L. Tang, Y. Fang and X. Tang, *J. Polym. Sci., Part A: Polym. Chem.*, 2005, **43**, 2921–2930.
32 Y. Chen, Z. Shen, H. Frey, J. Pérez-Prietob and S.-E. Stiriba, *Chem. Commun.*, 2005, 755–757.
33 R. Haag, *Angew. Chem., Int. Ed.*, 2004, **43**, 278–282.
34 Z.-L. Yu, F. Cheng, S.-J. Zhao, J.-W. Zhang, Z.-C. Cai and Y. Chen, *Macromol. Res.*, 2011, **19**, 189–196.
35 A. Sunder, M. Krämer, R. Hanselmann, R. Mülhaupt and H. Frey, *Angew. Chem., Int. Ed.*, 1999, **38**, 3552–3555.
36 D. Wan, Y. Lai, M. Jin and H. Pu, *Macromol. Chem. Phys.*, 2011, **212**, 1910–1917.
37 D. Wan, F. Chen, T. Kakuchi and T. Satoh, *Polymer*, 2011, **52**, 3405–3412.
38 D. Wan, H. Pu, M. Jin, G. Wang and J. Huang, *J. Polym. Sci., Part A: Polym. Chem.*, 2011, **49**, 2373–2381.
39 D. Wan, H. Pu, M. Jin, H. Pan and Z. Chang, *React. Funct. Polym.*, 2010, **70**, 916–922.
40 M. Calderón, M. A. Quadir, M. Strumia and R. Haag, *Biochimie*, 2010, **92**, 1242–1251.
41 X. Pang, L. Zhao, C. Feng and Z. Lin, *Macromolecules*, 2011, **44**, 7176–7183.
42 M.-C. Jones, M. Ranger and J.-C. Leroux, *Bioconjugate Chem.*, 2003, **14**, 774–781.
43 F. Wang, T. K. Bronich, A. V. Kabanov, R. D. Rauh and J. Roovers, *Bioconjugate Chem.*, 2005, **16**, 397–405.
44 H. Liu, Y. Chen, Z. Shen and H. Frey, *React. Funct. Polym.*, 2007, **67**, 156–164.
45 Y. Liang, D. Wan, X. Cai, M. Jin and H. Pu, *J. Polym. Sci., Part A: Polym. Chem.*, 2010, **48**, 681–691.
46 X. Li, Y. Qian, T. Liu, X. Hu, G. Zhang, Y. You and S. Liu, *Biomaterials*, 2011, **32**, 6595–6605.
47 S. Hecht and J. M. J. Fréchet, *Angew. Chem., Int. Ed.*, 2001, **40**, 74–91.
48 P. Furuta and J. M. J. Fréchet, *J. Am. Chem. Soc.*, 2003, **125**, 13173–13181.
49 E. Burakowska and R. Haag, *Macromolecules*, 2009, **42**, 5545–5550.
50 S. Xu, Y. Luo and R. Haag, *Macromol. Rapid Commun.*, 2008, **29**, 171–174.
51 A. Heise, J. L. Hedrick, C. W. Frank and R. D. Miller, *J. Am. Chem. Soc.*, 1999, **121**, 8647–8648.
52 N. Stavrouli, A. I. Triftaridou, C. S. Patrickios and C. Tsitsilianis, *Macromol. Rapid Commun.*, 2007, **28**, 560–566.
53 F. Wang, T. K. Bronich, A. V. Kabanov, R. D. Rauh and J. Roovers, *Bioconjugate Chem.*, 2008, **19**, 1423–1429.
54 W. Yuan, J. Yuan, S. Zheng and X. Hong, *Polymer*, 2007, **48**, 2585–2594.
55 X. Cao, Z. Li, X. Song, X. Cui, P. Cao, H. Liu, F. Cheng and Y. Chen, *Eur. Polym. J.*, 2008, **44**, 1060–1070.
56 P.-F. Cao, R. Xiang, X.-Y. Liu, C.-X. Zhang, F. Cheng and Y. Chen, *J. Polym. Sci., Part A: Polym. Chem.*, 2009, **47**, 5184–5193.
57 H. Liu, Z. Shen, S.-E. Stiriba, Y. Chen, W. Zhang and L. Wei, *J. Polym. Sci., Part A: Polym. Chem.*, 2006, **44**, 4165–4173.
58 C. Ternat, L. Ouali, H. Sommer, W. Fieber, M. I. Velazco, C. J. G. Plummer, G. Kreutzer, H.-A. Klok, J.-A. E. Månson and A. Herrmann, *Macromolecules*, 2008, **41**, 7079–7089.
59 C. Xia, X. Ding, Y. Sun, H. Liu and Y. Li, *J. Polym. Sci., Part A: Polym. Chem.*, 2010, **48**, 4013–4019.
60 S. Xu, Y. Luo and R. Haag, *Macromol. Biosci.*, 2007, **7**, 968–974.